Fission and quasifission modes in heavy-ion-induced reactions leading to the formation of Hs*

I. M. Itkis, E. M. Kozulin, M. G. Itkis, G. N. Knyazheva, A. A. Bogachev, E. V. Chernysheva, L. Krupa, Yu. Ts. Oganessian, and V. I. Zagrebaev
Flerov Laboratory of Nuclear Reactions, Joint Institute for Nuclear Research, 141980 Dubna, Russia

A. Ya. Rusanov
Institute of Nuclear Physics of the National Nuclear Center of Kazakhstan, 050032 Almaty, Kazakhstan

F. Goennenwein
Physikalisches Institut, Universitaet Tuebingen, D-72076 Tuebingen, Germany

O. Dorvaux and L. Stuttgé
Institut Pluridisciplinaire Hubert Curien and Université de Strasbourg, F-67037 Strasbourg, France

F. Hanappe
Université Libre de Bruxelles, CP229, B-1050 Bruxelles, Belgique

E. Vardaci
Istituto Nazionale di Fisica Nucleare and Dipartimento di Scienze Fisiche dell'Università di Napoli, Napoli, Italy

E. de Goés Brennand
Departamento de Fisica, Universidade Estadual da Paraiba, 58109-753 Campina Grande, Brasil
(Received 12 January 2011; revised manuscript received 25 April 2011; published 23 June 2011)

Mass and energy distributions of binary reaction products obtained in the reactions ^{22}Ne+^{249}Cf,^{26}Mg+^{248}Cm, ^{36}S+^{238}U, and ^{58}Fe+^{208}Pb have been measured. All reactions lead to Hs isotopes. At energies below the Coulomb barrier the bimodal fission of Hs*, formed in the reaction ^{26}Mg+^{248}Cm, is observed. In the reaction ^{36}S+^{238}U, leading to the formation of a similar compound nucleus, the main part of the symmetric fragments arises from the quasifission process. At energies above the Coulomb barrier fusion-fission is the main process leading to the formation of symmetric fragments for both reactions with Mg and S ions. In the case of the ^{58}Fe+^{208}Pb reaction the quasifission process dominates at all measured energies.

DOI: 10.1103/PhysRevC.83.064613 PACS number(s): 25.70.Jj, 25.70.Gh, 27.90.+b

I. INTRODUCTION

In reactions with heavy ions complete fusion and quasifission (QF) are competing processes [1–4]. The relative contribution of QF to the capture cross section becomes dominant for superheavy composite systems, and compound nucleus (CN) formation is hindered by the QF process. The balance between the two processes strongly depends on the entrance channel properties, such as mass asymmetry, deformation of interacting nuclei, collision energy, and the Coulomb factor Z_1Z_2.

It is known that in superheavy composite systems QF mainly leads to the formation of asymmetric fragments with mass asymmetry ∼0.4 [5]. This type of QF process, so-called asymmetric quasifission (QFasym), is characterized by asymmetric angular distributions in the center-of-mass system and thus fast reaction times (∼10^{-21} s) [2,6]. The total kinetic energy (TKE) for these fragments is observed to be higher than that for CN fission (CNF) [6,7] and hence this process is colder than CNF. Due to this reason shell effects in QF are more pronounced [7].

Besides the asymmetric component, also the symmetric component may be affected by the presence of the QF process. Consequently, the question of whether the symmetric fragments originate from CNF or QF processes arises. On the one hand, the angular distribution for all these mass-symmetric fragments is symmetric with respect to 90° in the center-of-mass system and the estimated reaction time is ∼10^{-20} s, typical for CNF processes [2,8]. On the other hand, the calculations of potential energy surfaces for heavy-ion-induced reactions along with Langevin-type dynamic equations of motion show [9] that one of the possible reaction channels for such systems is a process occurring without a CN stage, but with fragment properties close to those known from CNF. This process is characterized by long reaction times sufficient for mass equilibration and resulting in the formation of symmetric fragments [symmetric quasifission (QFsym)]. In Fig. 1 a potential energy surface for a heavy-ion-induced reaction leading to a superheavy composite system as a function of elongation and mass asymmetry is shown. The solid lines with arrows trace schematically (without fluctuations) the most probable trajectories. However, when in the reactions with heavy ions nuclei come in contact, they will become excited, and fluctuations play an important role in the further evolution of the composite system. Due to these fluctuations, fragments

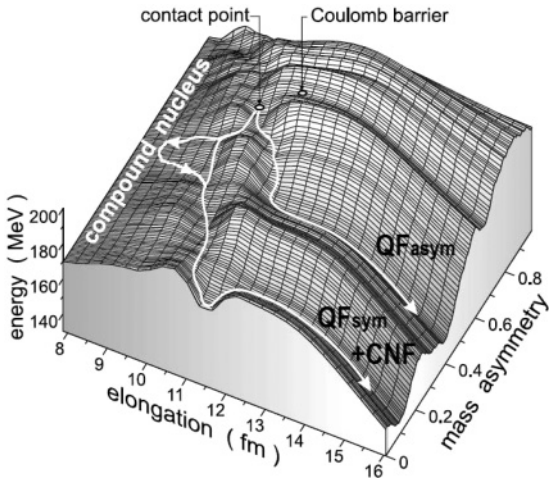

FIG. 1. Example of a driving potential energy surface as a function of elongation and mass asymmetry for a heavy-ion-induced reaction leading to a superheavy composite system taken from Ref. [10].

formed in the QFasym process could, with some probability, thus have masses close to symmetry.

To explore the relative contributions of CNF and QF to symmetric splitting we have investigated binary reaction channels of the composite systems with $Z = 108$ produced in reactions with ^{22}Ne, ^{26}Mg, ^{36}S, and ^{58}Fe ions at energies below and above the Bass barrier. The entrance channel properties of these systems are presented in Table I. It is important to note that all reaction partners, except ^{208}Pb, are well-deformed nuclei. In the reactions with deformed nuclei the potential energy surface strongly depends on the relative orientation of the reaction partners. Except for reactions with pronounced mass asymmetry in the entrance channel, the dominance of tip configurations at energies below the barrier leads to the increase of QF contributions [11–13].

This paper presents the detailed analysis of mass and TKE distributions of fissionlike fragments for the reactions ^{22}Ne+^{249}Cf,^{26}Mg+^{248}Cm, ^{36}S+^{238}U, and ^{58}Fe+^{208}Pb. A similar experimental study of binary fragments of the composite systems ^{264,270,271,272}Hs* exited well above the Bass barrier was performed in Ref. [16] for the reactions ^{22}Ne+^{249}Cf, ^{32}S+^{238}U, ^{40}Ar+^{232}Th, and ^{56}Fe+^{208}Pb. The reaction ^{34}S+^{238}U was already studied in Ref. [17]. Since the relative contributions of CNF and QF depend on the energy of the interacting nuclei, we have measured the mass-energy distributions of binary fragments for the studied reactions at energies below and above the Bass barrier. Special attention is paid to the properties of symmetric fragments in order to assign probabilities of CNF and QF processes.

TABLE II. The positions of the arms of the CORSET spectrometer and their acceptance angles for the reactions studied.

Reaction	θ_1 (deg)	θ_2 (deg)	Acceptance (deg)
^{22}Ne+^{249}Cf	58	100	±22
^{26}Mg+^{248}Cm	60	95	±20
^{36}S+^{238}U	67	67	±12
^{58}Fe+^{208}Pb	60	60	±20

II. EXPERIMENT

The experiments were carried out at the Flerov Laboratory of Nuclear Reactions using beams of ^{22}Ne, ^{26}Mg, ^{36}S, and ^{58}Fe ions extracted from the U-400 cyclotron at energies around the Coulomb barrier. The energy resolution was ∼2%. Beam intensities on targets were 1–2 pnA. Layers of ^{208}Pb, ^{238}UF$_4$, ^{248}Cm, and ^{249}Cf, 120–200 μg/cm^2 thick, deposited on a 40–50 μg/cm^2 carbon backings, were used as targets. The enrichment was 99.99%. During the experiment the carbon backing faced the beam.

Binary reaction products were detected in coincidence by the two-arm time-of-flight spectrometer CORSET [18]. Each arm of the spectrometer consists of a compact start detector and a position-sensitive stop detector, both based on microchannel plates. The arms of the spectrometer were positioned in an optimal way according to the kinematics of the reactions. The arm angles and acceptances for each studied reaction are presented in Table II. In the case of S- and Fe-induced reactions the scission axis for symmetric splitting is orthogonal to the beam axis at the angles chosen for the CORSET arms. Due to large correlation angles between the fragment pairs for the reactions induced by Ne and Mg ions, the arms of the spectrometer were positioned asymmetrically. The distance between the start and stop detectors was 12–15 cm. The start detectors were placed at a distance of 3–5 cm from the target. A

TABLE I. Properties of the systems, leading to the Hs* compound nuclei, studied in this paper. A_{CN} is the CN atomic mass number; $\eta_0 = (A_t - A_p)/(A_t + A_p)$ is the entrance channel mass asymmetry. β_2 is the deformation parameter for the projectile and target nuclei, as deduced from the electric quadrupole transition probability between the first 2^+ state and 0^+ ground state [14]. B_{Bass} is the Bass barrier in the center-of-mass system; B_{tip} and B_{side} are the barriers for tip and side configurations, respectively [15].

Reaction	A_{CN}	η_0	Z_1Z_2	β_2 deformation		B_{Bass}	B_{tip}	B_{side}
				projectile	target	(MeV)	(MeV)	(MeV)
^{22}Ne+^{249}Cf	271*	0.838	980	0.562	0.299[a]	108.98	94.68	118.96
^{26}Mg+^{248}Cm	274*	0.810	1152	0.482	0.297	126.82	111.64	138.76
^{36}S+^{238}U	274*	0.737	1472	0.168	0.286	159.08	147.53	170.79
^{58}Fe+^{208}Pb	266*	0.564	2132	0.259	0	227.15	224.35	240.67

[a]The deformation is taken for ^{250}Cf (no data for ^{249}Cf).

typical mass resolution of the spectrometer in these conditions is ∼2–3 u.

The data processing assumes standard two-body kinematics [18]. Primary masses, velocities, energies, and angles in the center-of-mass system of reaction products were calculated from measured velocities and angles in the laboratory system using the momentum and mass conservation laws with the assumption that the mass of the composite system is equal to $M_{\text{target}}+M_{\text{projectile}}$. Neutron evaporation before scission is not taken into account. This is justified by the fact that even at the highest reaction energies not more than four neutrons could be emitted. Hence, considering that the spectrometer resolution is 2–3 u, the neutron emission will not lead to visible effects on the mass-energy distributions. Fragment energy losses in the target, backing, and the start detector foils were taken into account.

The identification of the binary reaction channel with full momentum transfer (FMT) and the removal of products of sequential and incomplete fission reactions, induced fission of target and targetlike nuclei, or reactions on impurity atoms in the target was based on the analysis of the kinematic diagram (the velocity vectors of two detected reaction products) in the center-of-mass system [11]. For FMT events the distribution of the $V_\perp$ component of fragment velocity (projection of the fragment velocity vector onto the plane perpendicular to the beam) is expected to peak at zero, while the $V_\parallel$ (projection of the fragment velocity vector onto the beam axis) should be equal to the calculated center-of-mass velocity for the collision $V_{\text{c.m.}}$. Figure 2 illustrates the extraction of FMT events in the reaction ^{26}Mg+^{248}Cm at $E_{\text{lab}} = 129$ MeV. From this figure, it is apparent that the spectrometer detects three main groups of events. The events for which $V_\parallel$ is equal to $V_{\text{c.m}}$ correspond to the binary products of the reaction ^{26}Mg+^{248}Cm, while the groups of events with $V_\parallel$ lower and higher than $V_{\text{c.m}}$ correspond to spontaneous fission of the target nucleus and reactions on impurity atoms in the target. The contour in Fig. 2 accepts 99% of FMT events ($\pm 3\sigma$), but removes a substantial fraction of interfering processes. The remaining background is at most a few percent of the FMT yield.

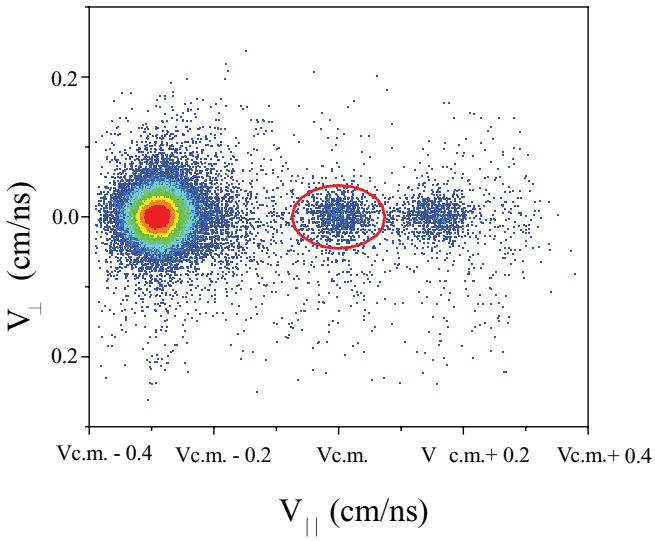

FIG. 2. (Color online) The distribution of velocity components $V_\parallel$ and $V_\perp$ for the reaction ^{26}Mg+^{248}Cm at a beam energy of 129 MeV. $V_\parallel$ is plotted relative to the calculated center-of-mass velocity $V_{\text{c.m.}}$.

III. RESULTS AND DISCUSSION

Figures 3–6 display the measured TKE-mass distributions of the binary fragments for the reactions ^{22}Ne+^{249}Cf, ^{26}Mg+^{248}Cm, ^{36}S+^{238}U, ^{58}Fe+^{208}Pb, respectively. In the TKE-mass matrix the reaction products with masses close to those of the projectile and target are associated with quasielastic and deep-inelastic events. They were not considered in the present analysis. Reaction products lying between quasielastic peaks are assumed to originate either from CNF or QF processes. The events selected are those within the

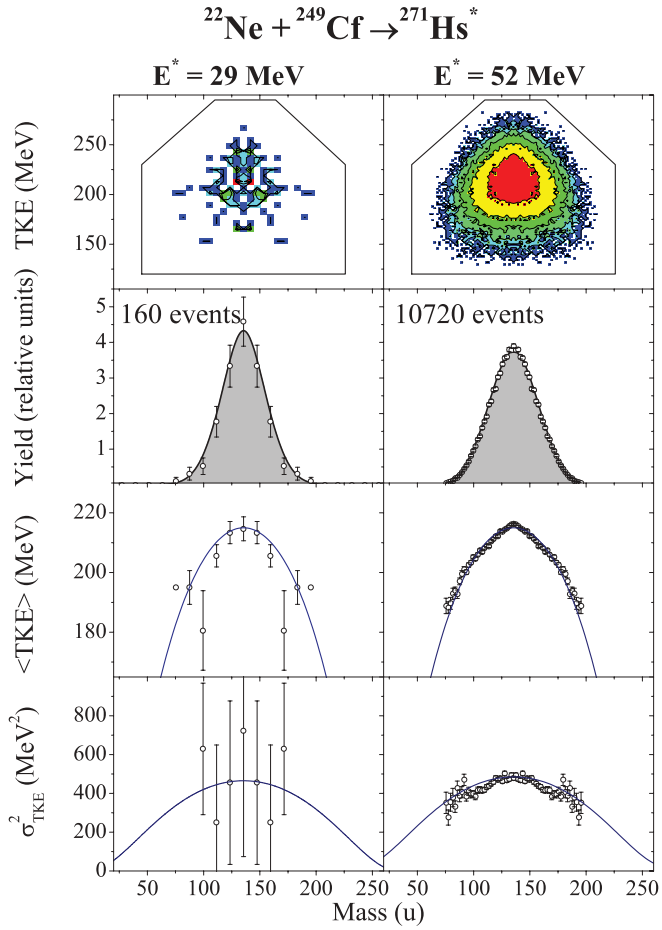

FIG. 3. (Color online) The mass-energy distributions of binary products for the ^{22}Ne+^{249}Cf reaction at projectile energies 102 and 127 MeV corresponding to excitation energies of CN of 29 and 52 MeV, respectively [from top to bottom: the (TKE, M) matrices for binary products; the mass yields; the average total kinetic energy and its dispersion as a function of mass for fissionlike fragments inside the outlined contour on the (TKE, M) matrices]. The total statistics for fragments inside the contours on the (TKE, M) matrices are indicated at the top of mass yield plots. Filled areas in the mass distributions are associated with CNF (see text). Solid lines in the average TKE and dispersion of the TKE distributions delineate the expectation from the LDM.

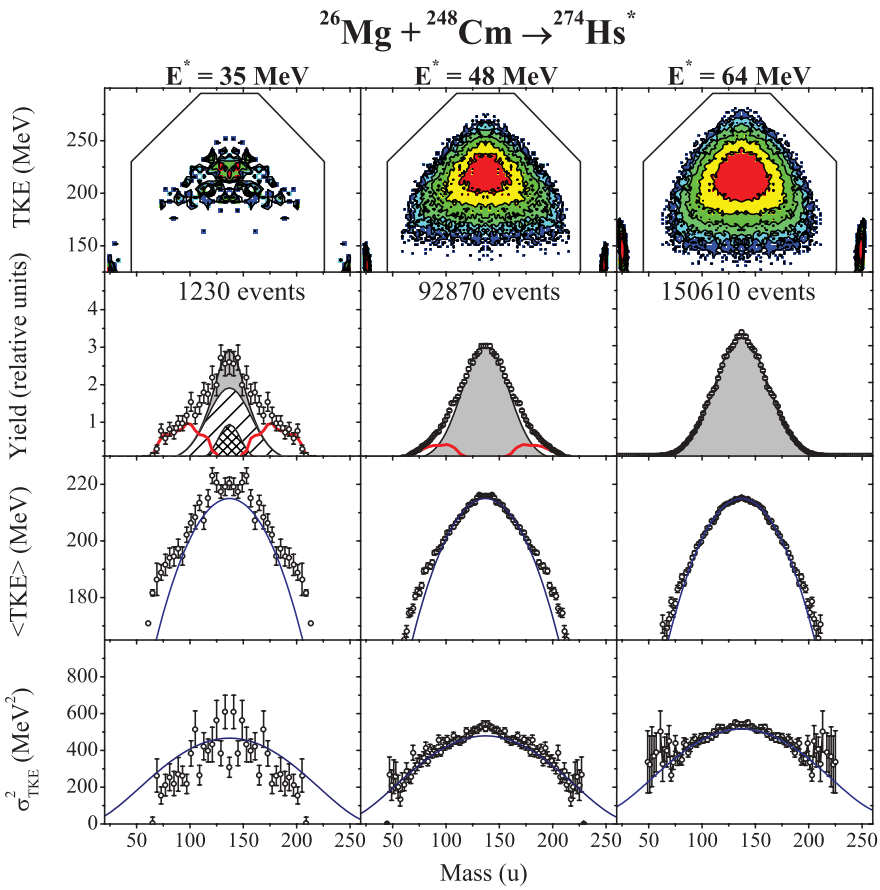

FIG. 4. (Color online) Same as Fig. 3, but for the ^{26}Mg+^{248}Cm reaction at projectile energies 129, 143, and 160 MeV corresponding to CN excitation energies of 35, 48, and 64 MeV, respectively. The sparsely and densely hatched regions in the mass distribution at an excitation energy of 35 MeV correspond to low- and high-energy components of bimodal fission, respectively (see Fig. 7). Thick solid lines in the mass distributions correspond to QF.

contour lines in the TKE-mass distributions in Figs. 3–6. The respective mass distributions, average TKEs, and dispersions of the TKE are presented in the lower panels of the figures.

Even at similar CN excitation energies the mass-energy distributions are vastly different for these reactions. In the case of the reactions ^{22}Ne+^{249}Cf and ^{26}Mg+^{248}Cm, at energies above the Coulomb barrier, a near Gaussian form of the mass distributions indicates that the fragments are produced by a CNF process as predicted by the liquid drop model (LDM) in the case of relatively hot nuclei. This conclusion is supported by the trend in $\langle \mathrm{TKE} \rangle$ and σ^2_{TKE}. However, at lower values of excitation energy, where the deviation from a Gaussian shape is evident, some traces of asymmetric fission are observed.

For the ^{36}S+^{238}U reaction the mass distributions of the fissionlike fragments change markedly. At low excitation energies the mass distributions are dominantly asymmetric. A symmetric peak appears with growing intensity as the excitation energy is increased. At higher excitation energies the mass distribution becomes symmetric and similar to the reaction ^{26}Mg+^{248}Cm, though slightly wider. As supported by the conclusions drawn in Refs. [5,6,13], we attribute the asymmetric component of mass distribution to the QF process. We may reasonably assume that this difference in mass distributions for the ^{26}Mg+^{248}Cm and ^{36}S+^{238}U reactions is connected with an increasing contribution of the QF process for the ^{36}S-induced reaction. The obtained mass distributions for the ^{36}S+^{238}U reaction are in good agreement with data from Ref. [19], where only fragment mass distributions and fission cross sections were measured. The procedure to deconvolute the CNF component from this three-humped distribution will be discussed in the next section.

In the case of the ^{58}Fe+^{208}Pb reaction, the mass-energy distribution has a wide U shape even at an exitation energy of 48 MeV. For this reaction the QF process dominates at energies below and above the Bass barrier. The strong overlap between QF fragments, and quasielastic and deep-inelastic events is observed due to the fact that one of the partners is doubly magic lead.

Some noteworthy features of the QFasym component of fragment mass distributions for the studied reactions can be highlighted at this point. Generally, in heavy-ion-induced reactions the formation of QFasym fragments is connected with the strong influence of the nuclear shell at $Z = 82$ and $N = 126$ (doubly magic lead). In fact, as was shown in Ref. [20], for the ^{48}Ca+^{238}U reaction the maximum yield corresponds to fragments with masses 208 u. However, in reactions with lighter projectiles on a uranium target, the asymmetric QF peak shifts toward more symmetric masses [21]. By contrast, for the heavier projectile ^{64}Ni, the maximum yield of QFasym fragments corresponds to the heavy mass 215 u [20]. This trend is illustrated in Table III, where the positions of heavy QF fragments for these reactions are presented. But, in the formation of the asymmetric QF component, also the closed shell in the light fragment at $Z = 28$ and $N = 50$ could be effective, together with the shells $Z = 82$ and $N = 126$, and could lead to a shift of the asymmetric QF peak. Based on the simple assumption of an N/Z equilibration, the masses of the light and heavy fragments corresponding to these closed shells

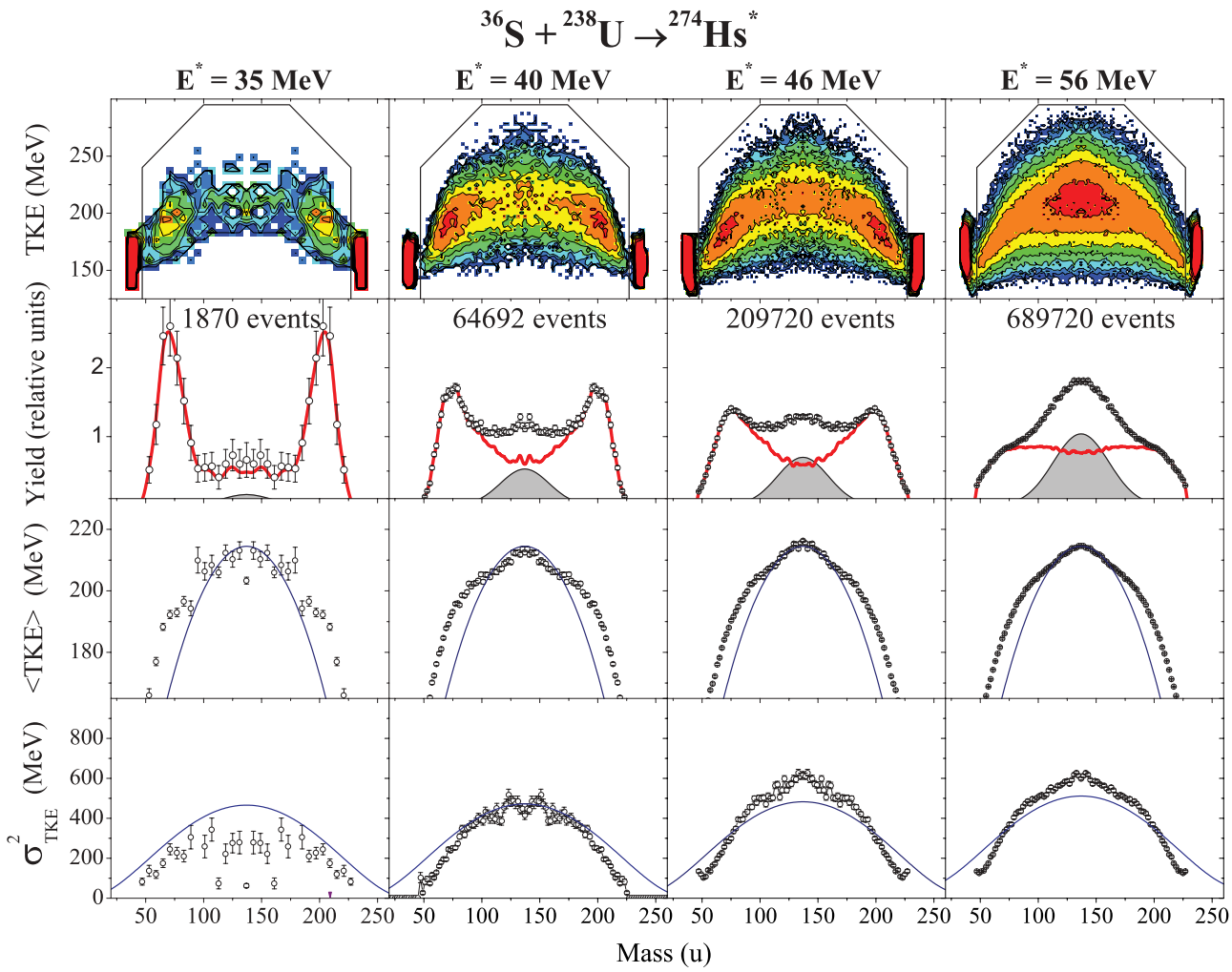

FIG. 5. (Color online) Same as Fig. 3, but for the ^{36}S+^{238}U reaction at projectile energies 173, 179, 186, and 198 MeV corresponding to CN excitation energies of 35, 40, 46, and 56 MeV, respectively. Note the strong contribution of asymmetric QF seen both in the mass yield and the energy as a function of mass.

were calculated. In Table III $M_{\mathrm{H}}^{\mathrm{Shell}}$ is a heavy fragment mass averaged over all these shells. The obtained values of $M_{\mathrm{H}}^{\mathrm{Shell}}$ are in good agreement with the experimental ones, except for the more asymmetric ^{26}Mg+^{248}Cm and ^{30}Si+^{238}U reactions. For these reactions the Coulomb repulsion is expected to be smaller. This may lead to longer reaction times before separation for asymmetric QF and thus allow for larger numbers of nucleons to be exchanged. For the other more symmetric reactions with heavier projectiles, the major part of the asymmetric QF peak fits into the region of the $Z = 82$, $N = 126$ and $Z = 28$, $N = 50$ shells. The maximum yield of the asymmetric QF component is a mixing between all these shells.

A. Analysis of the mass distributions

The width of the fission fragment mass distributions could be an indicator for the presence of QF in fissionlike mass

TABLE III. Positions of heavy peaks in the primary mass distributions of QFasym fragments in reactions with heavy ions.

Reaction	Z_1Z_2	M_{H}	$M_{\mathrm{H}}^{\mathrm{Shell}}$	Exchanged nucleons	Reference
^{26}Mg+^{248}Cm	1152	180	202.5	68	This work
^{30}Si+^{238}U	1288	178	199.3	60	Nishio *et al.* [21]
^{36}S+^{238}U	1472	200	202.5	38	This work, Nishio *et al.* [21]
^{40}Ar+^{238}U	1656	204	204.5	34	Nishio *et al.* [21]
^{48}Ca+^{238}U	1840	208	208.5	30	Kozulin *et al.* [20]
^{64}Ni+^{238}U	2576	215	216.5	23	Kozulin *et al.* [20]

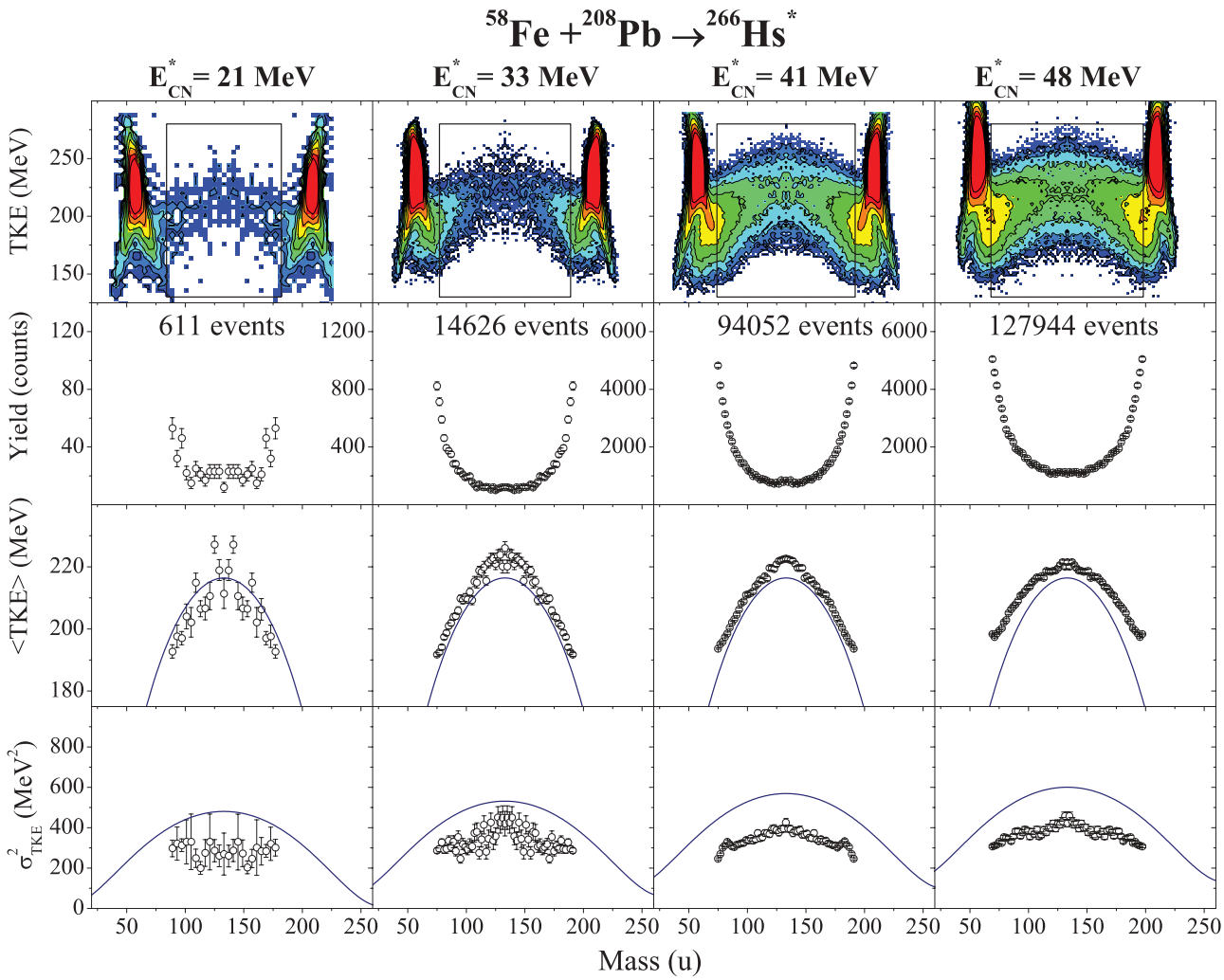

FIG. 6. (Color online) Same as Fig. 3, but for the ^{58}Fe+^{208}Pb reaction at projectile energies 289, 305, 315, and 324 MeV corresponding to CN excitation energies of 21, 33, 41, and 48 MeV, respectively.

spectra. A strong increase in the width of mass distributions is observed for reactions leading to highly fissile compound nuclei in going from quite asymmetric to less asymmetric combinations of the reaction partners in the entrance channel [3,22]. For the analysis the properties of CNF are exploited in the framework of the LDM to spot the contribution of CNF in the reactions. The basic equations and the expected characteristics of mass and energy distributions for CNF are presented in the following.

In general, the width of the mass distributions for fission processes depends on the excitation energy and angular momentum of the CN. In a first approximation [23], the dispersion σ_M^2 increases linearly with $\langle l^2\rangle$ and with nuclear temperature T, and can be written as

$$\sigma_M^2 = \frac{\partial\sigma_M^2}{\partial T}T + \frac{\partial\sigma_M^2}{\partial l^2}\langle l^2\rangle. \qquad (1)$$

The first term in Eq. (1) corresponds to the dispersion of mass distributions at zero angular momentum and can be calculated (with some assumptions) as

$$\frac{\partial\sigma_M^2}{\partial T}T = \frac{A_{\rm CN}^2 T}{16}\left[\left(\frac{d^2V}{d\eta^2}\right)_{\eta=0}\right]^{-1}, \qquad (2)$$

where $(\frac{d^2V}{d\eta^2})_{\eta=0}$ is the second derivative of the potential energy of the deforming nucleus with respect to mass-asymmetric deformations $\eta = \frac{4}{A_{\rm CN}}(M - A_{\rm CN}/2)$ at the saddle point taken for symmetric mass split and at zero angular momentum. The sensitivity of the dispersion to angular momentum is much weaker, although not negligible, especially in the case of S- and Fe-ion-induced reactions. For the estimates of the coefficients $(d^2V/d\eta^2)_{\eta=0}$ and $\partial\sigma_M^2/\partial l^2$ we used the corresponding systematics presented in Ref. [23]. The saddle-point temperatures, angular momenta, and dispersions of mass distributions of fission processes for the systems studied in the present work are listed in Table IV.

The mass distributions were fitted by Gaussians with the dispersions given in Table IV. These fits are displayed as solid lines in Figs. 3–6. The Gaussian fit procedure is

TABLE IV. Energy-dependent characteristics for the reactions studied. $E_{\mathrm{c.m.}}$ is the energy in the center-of-mass system. E^* is the CN excitation energy calculated with the ground-state masses [24], $\langle l \rangle$ is the CN mean angular momentum calculated using the nuclear reaction vision project [15], T_{saddle} is the saddle-point temperature, σ_M is the standard deviation of mass distributions calculated according to Eq. (1), and σ_{TKE} is the standard deviation of TKE distributions calculated according to Ref. [23].

E_{lab} (MeV)	$E_{\mathrm{c.m.}}$ (MeV)	E^* (MeV)	$\langle l \rangle$ ($\hbar$)	T_{saddle} (MeV)	σ_M (u)	σ_{TKE} (MeV)
			^{22}Ne+^{249}Cf			
102	93.7	29	7	0.98	19.5	21.3
127	116.7	52	22	1.13	22.1	21.7
			^{26}Mg+^{248}Cm			
125	113.1	32	8	1.01	20.1	21.3
129	116.8	35	9	1.03	20.3	21.4
143	129.4	48	19	1.11	21.8	21.6
160	144.8	64	35	1.18	24.4	22.5
			^{36}S+^{238}U			
168	145.9	31	9	1.00	20.0	21.3
173	150.3	35	11	1.03	20.4	21.4
179	155.5	40	15	1.06	21.0	21.5
186	161.6	46	22	1.10	22.0	21.7
198	172.0	56	33	1.15	24.0	22.4
			^{58}Fe+^{208}Pb			
289	226.0	21	16	0.93	19.3	21.5
297	232.2	27	26	0.99	20.1	21.9
305	238.5	33	37	1.04	23.2	22.7
315	246.3	41	47	1.09	25.6	23.5
324	253.3	48	54	1.14	27.4	24.1

straightforward for the cases of Ne and Mg ions at high CN excitation energies (∼50 MeV), where the influence of shell effects is negligible and the fission process is well described by the LDM. A large uncertainty arises in the fitting procedure for the reaction S+U at all energies due to large contributions by the QF process. To make this procedure more definite, we analyzed simultaneously the TKE distributions and their dispersions for fissionlike fragments for all studied reactions. The Fe-induced reaction is discussed in Sec III B.

B. Analysis of the TKE distributions

It is well known that the kinetic energy of fission fragments is mainly determined by the Coulomb repulsion of fragments formed at the scission point of the CN. In the framework of the LDM, the average kinetic energy has a parabolic dependence on the fragment mass [25] and practically does not depend on the excitation energy and angular momentum of the CN. Such behavior of the TKE is confirmed by experimental data. We used the Viola systematics based on experimental data as a function of the $Z^2/A_{\mathrm{CN}}^{1/3}$ parameter [26] to estimate the most probable TKE of CNF. However, we must remark that in more recent systematics the data from Ref. [2] measured at energies well above the Coulomb barrier were included. In these reactions a considerable amount of QF processes contributes to the fission products. It turns out that the older systematics of Viola [27], without taking into account the experimental data from Ref. [2], provides a lower value of TKE, which is more appropriate for the CNF process. Moreover, in the case of CNF at excitation energies of CN higher than 40 MeV, the TKE distribution of the partner fragments is independent of the excitation energy and exhibits a typical Gaussianlike shape.

According to the LDM suggested by Nix and Swiatecki in Ref. [25], the dependences of the average TKE and its variance on mass can be presented as follows:

$$\langle \mathrm{TKE} \rangle(M) = \langle \mathrm{TKE} \rangle(A_{\mathrm{CN}}/2)[1-(\eta/2)^2][1+\alpha(\eta/2)^2], \quad (3)$$

$$\langle \mathrm{TKE} \rangle^2(M)/\sigma_{\mathrm{TKE}}^2(M) = \mathrm{const}. \quad (4)$$

The parameter α characterizes the degree of deviation of $\langle \mathrm{TKE} \rangle(M)$ from the parabolic dependence.

According to calculations in the framework of the stochastic approach to the fission dynamics based on three-dimensional Langevin equations, the variance of the TKE distribution depends on the angular momentum of the CN [28]. For heavy fissioning nuclei $d\sigma_{\mathrm{TKE}}^2/dl^2 > 0$, and for medium and light fissioning nuclei $d\sigma_{\mathrm{TKE}}^2/dl^2$ is also positive for high angular momenta, while for low angular momenta σ_{TKE}^2 decreases with increasing l^2. The compilation of the experimental data at excitation energies of the CN of ∼40–50 MeV [23] in fact shows that the TKE dispersion practically does not change for compound nuclei with $Z^2/A_{\mathrm{CN}}^{1/3}$ up to ∼1000 and increases linearly for heavier CN. According to this systematics, values of ∼450 MeV^2 for the TKE dispersion and $d\sigma_{\mathrm{TKE}}^2/dl^2 \approx 0.04$ are expected for the Hs nuclei. The estimated values of σ_{TKE} are listed in Table IV. The solid curves on the $\langle \mathrm{TKE} \rangle$ and σ_{TKE}^2 plots in Figs. 3–6 are the descriptions of the LDM component with the dependences derived from Eqs. (3) and (4).

For the reactions induced by ^{22}Ne and ^{26}Mg ions at high excitation energies of the CN, the mass distributions are well described by a single Gaussian, and the average TKEs and their variances agree well with the calculations using Eqs. (3) and (4). Consequently, the properties of the fragments in the reactions ^{22}Ne+^{249}Cf and ^{26}Mg+^{248}Cm are close to the prediction of the LDM at high excitation energies of compound nuclei and may hence be attributed to CNF processes.

However, for the ^{26}Mg+^{248}Cm reaction at an excitation energy of 35 MeV of the CN, some deviations from LDM predictions are observed for fragments, both symmetric and asymmetric. The increased yields of fragments with masses 70–100 u may be caused by the QF process since the interaction energy is ∼10 MeV less than the Bass barrier, and the orientation effects on the reaction dynamics become apparent at this energy. It should be mentioned that possibly this increase of yields can also be attributed to superasymmetric fission which is caused by shell effects in light fragments [29]. The average TKE is higher in this mass region compared to the parabolic dependence of Eq. (3). This is linked to shell effects.

The TKE of symmetric fragments is also higher than predicted. In Fig. 7 the TKE distributions are shown for symmetric fragments with masses $A_{CN}/2\pm20$ u obtained in the ^{22}Ne+^{249}Cf and ^{26}Mg+^{248}Cm reactions at two excitation energies of the compound nuclei (below and above the Bass barrier). It is readily seen that the TKE distributions have a complex structure at low excitation energy, while at high excitation energy they are well described by single Gaussians with parameters coming from the LDM.

At low excitation shell effects show up in the CNF process, giving rise to a structure in the mass-energy distributions of fission fragments. The structural features of the TKE distributions at low excitation may arise due to the fact that in symmetric fission both fragments are close to the spherical neutron shells with $N = 82$. A similar behavior could be observed when both fission fragments are close to the spherical proton shell $Z = 50$. In fact, the phenomenon of bimodality has been disclosed in the case of spontaneous and low-energy fission of nuclei in the Fm-Rf ($Z = 100$–104) region.

Bimodal fission was discovered in the 1980's by Hulet and collaborators [30]. Some spontaneously fissioning isotopes of Fm, Md, and No were found to exhibit symmetric fragment mass distributions, whose widths are changing very rapidly from nucleus to nucleus. For example, for spontaneous fission of ^{258}Fm the mass distribution is unusually narrow, while for the neighboring nucleus ^{259}Md with only one more proton it is rather broad. Even more spectacular are the distributions of TKE, which are double humped. The two humps are centered at $\langle$TKE$\rangle \approx 200$ MeV and an unexpectedly large $\langle$TKE$\rangle \approx 230$ MeV, respectively. This feature led to the notion of two distinct symmetric fission modes, one at low TKE and one at high TKE. At closer inspection it is observed that the high-energy mode is linked to a narrow mass distribution while the low-energy mode has a wide mass distribution. The name given to this phenomenon was bimodal symmetric fission. By theory, bimodal fission is explained by the existence of two different paths on the potential energy surface leading to fission [31,32]. One path is described by the LDM, while for

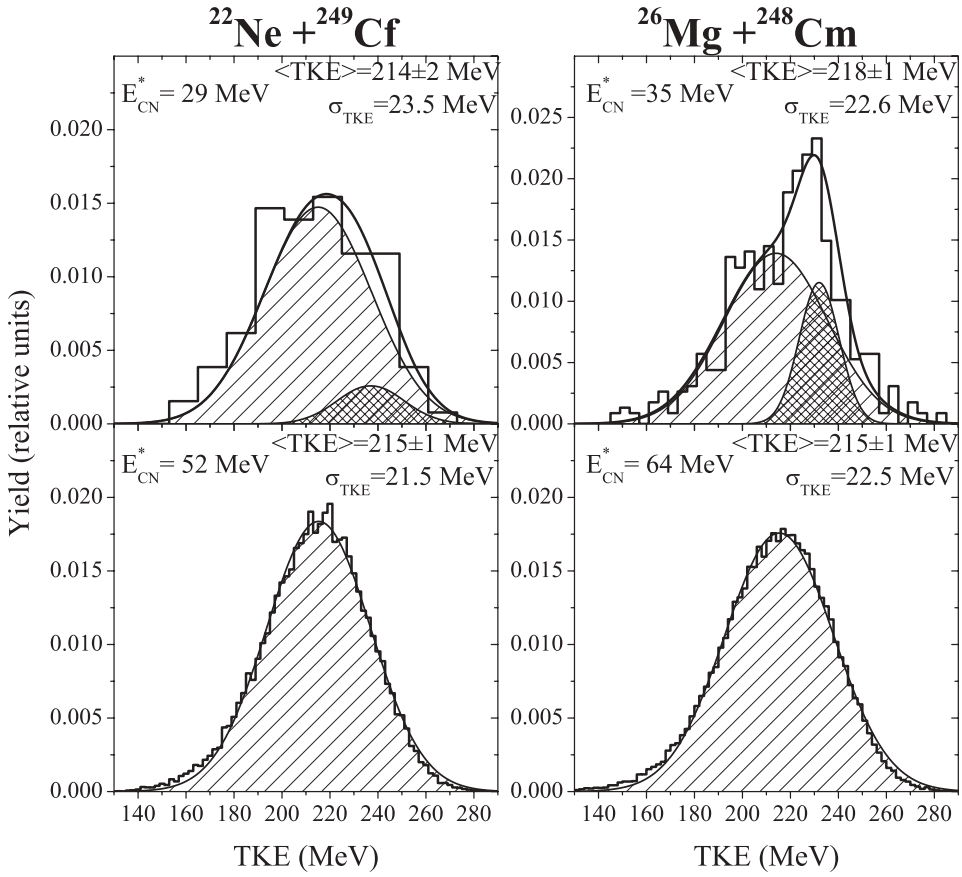

FIG. 7. TKE distributions of fragments with masses $A_{CN}/2\pm20$ u for the reactions ^{22}Ne+^{249}Cf (left-hand panel) and ^{26}Mg+^{248}Cm (right-hand panel). Mean values and standard deviations of the experimental TKE distributions are indicated in the top right-hand corner of each plot. High and low kinetic energy components are given as densely and sparsely hatched regions, respectively.

the other path shell effects play an important role. The LDM path leads to elongated scission configurations while the shell effect path corresponds to compact configurations. Since by far most of the final TKE is due to the Coulomb repulsion between fragments following scission, the shape elongation of the scission configuration determines the TKE. Hence, high and low TKE for the two paths is rapidly understood. Both paths result in symmetric (or nearly so) mass distributions, but the high TKE valley is narrower while the low TKE valley is much wider. This explains the difference in width of the mass distributions. It has become customary to call the high TKE and narrow mass width mode "symmetric compact fission" and the low TKE and broad mass width mode "symmetric elongated fission" [33].

Returning to the TKE distributions of symmetric fragments of the ^{26}Mg+^{248}Cm at subbarrier energies, one can see in Fig. 7 that they may be deconvoluted into two Gaussians, the constituent peaks lying near ∼214 and ∼230 MeV. Only the lower energy corresponds to the established linear dependency of the TKE on the Coulomb parameter $Z^2/A_{\rm CN}^{1/3}$ in the LDM. Hence, for the reaction Mg+Cm leading to ^{274}Hs*, bimodal fission is observed.

In the case of the ^{22}Ne+^{249}Cf reaction the standard deviation of the experimental TKE distribution is higher for the lower energy. This is in contradiction to single-mode LDM fission. Thus, we have some evidence for bimodal fission at an excitation energy of 29 MeV, although due to lack of statistics the decomposition of the TKE distribution is not fully obvious. It is important to note the enhanced relative contribution of the high-energy component in the case of ^{274}Hs* fission (^{26}Mg+^{248}Cm reaction) as compared to ^{271}Hs* fission (^{22}Ne+^{249}Cf reaction), in spite of the fact that the excitation energy is higher for the Mg-induced reaction. At symmetric fission of ^{274}Hs* both fragments have $N = 83$, while in the case of ^{271}Hs* the neutron number N is 81.5. According to the systematics for pre- and postscission neutron emission accompanying fission [34], values of 1.1 and 0.6 prescission neutrons are expected for ^{274}Hs* ($E^* = 35$ MeV) and ^{271}Hs*($E^* = 29$ MeV), respectively. Thus the formation of two spherical fragments with a neutron number $N = 82$ is more favorable in the case of ^{274}Hs* as compared to ^{271}Hs*.

In the right-hand panel of Fig. 8 the TKE distributions of the symmetric fragments obtained in the reaction ^{58}Fe+^{208}Pb are presented. The mean TKE increases with increasing projectile energy. According to the Viola systematics, the mean TKE value for the CNF of ^{266}Hs* is expected to be 216 MeV, whereas we obtained values of 211±2 MeV at $E^* = 21$ MeV and 220±1 MeV at $E^* = 48$ MeV. The TKE distributions are narrower than expected for the CNF, and their standard deviations virtually do not depend on projectile energy. We trace the increase of the TKE to the QF process. The reason for this is the following: It is well known that for CNF processes the shell effects fade away when the excitation energy increases, and hence kinetic energies decrease, as we observed in the case of the ^{26}Mg+^{248}Cm reaction. But for the reaction ^{58}Fe+^{208}Pb the situation is reversed due to the fact that the QF process is colder than CNF, and shell effects play a dominant role for this process even at high excitation energies. Moreover, for this reaction the dispersion of the TKE virtually does not depend on the mass of the reaction fragments at all measured energies (see Fig. 6) with average of ∼300 MeV^2, which is significantly smaller than that expected from experimental systematics for the CNF [23]. For the ^{58}Fe+^{208}Pb reaction QF is a dominant process at all energies, with TKE dispersions smaller than those for CNF.

As opposed to the ^{26}Mg+^{248}Cm reaction where CNF is the main process, and to the ^{58}Fe+^{208}Pb reaction where QF predominates, in the case of the reaction ^{36}S+^{238}U both CNF and QF contribute significantly. The mean value and dispersion of TKE increase with increasing energy of ^{36}S ions and exceed the LDM predictions at the highest energy. This is clearly seen in Fig. 5. The TKE distributions of fragments formed in the reaction with ^{36}S ions at energies above and below the Coulomb barrier for symmetric mass splits are shown in the left-hand panel of Fig. 8. At an excitation energy of 56 MeV the TKE distribution seems to be a simple Gaussian. But the standard deviation is higher than that from the LDM, whereas in the reactions with Mg and Ne ions at the high excitation energies the TKE distributions are well described by a single Gaussian with the parameters coming from the LDM. One may speculate about the presence of other processes together with the CNF in the symmetric mass region for the ^{36}S+^{238}U reaction. We assume that the mass symmetric fragments may be formed by three different modes: CNF, symmetric QF, and a tail of the asymmetric QF process. To evaluate the contribution of the CNF process in the symmetric mass region, the TKE distributions are decomposed as a sum of three Gaussians. One of them is associated with the CNF process (filled region in Fig. 8). For the excitation energies 40 and 56 MeV we fix the mean value and variance of this component to the values predicted from the systematics presented in Refs. [26] and [23], respectively. The low-energy component in Fig. 8 is attributed to QFasym while the high-energy one is connected with QFsym. The yield of CNF fragments in the mass distribution being described by a Gaussian (see the previous section) was weighted using this estimation. The mass decomposition is shown in Fig. 5. It should be noted that our results agree well with the calculations based on a dynamical description using the Langevin equation [17], in which the mass distributions for CNF and QF fragments were separately determined for the similar reaction ^{34}S+^{238}U.

As it was mentioned above, the reaction ^{36}S+^{238}U leads to the formation of a similar CN as in the reaction ^{26}Mg+^{248}Cm. But the TKE distributions for these reactions are different, in particular, at the lowest excitation energy of 35 MeV. In the case of the S-induced reaction, the TKE distribution is narrower and shifted to lower energies with the mean value of the TKE being 210 MeV as compared to 218 MeV for the Mg-induced reaction. A similar narrower TKE distribution with a lower mean value was observed for the reaction ^{58}Fe+^{208}Pb for which QF is a dominant process. Since in CNF the properties of the same CN formed in different reactions at the same excitation energy do not change (neglecting small differences in angular momentum of the compound nucleus after its formation), this shift of the TKE in the ^{36}S+^{238}U→^{274}Hs* reaction must be due to a large contribution of QF in the fragment mass region $A_{\rm CN}/2$±20 u. Since for the same CN ^{274}Hs* formed in the Mg-induced reaction bimodal fission

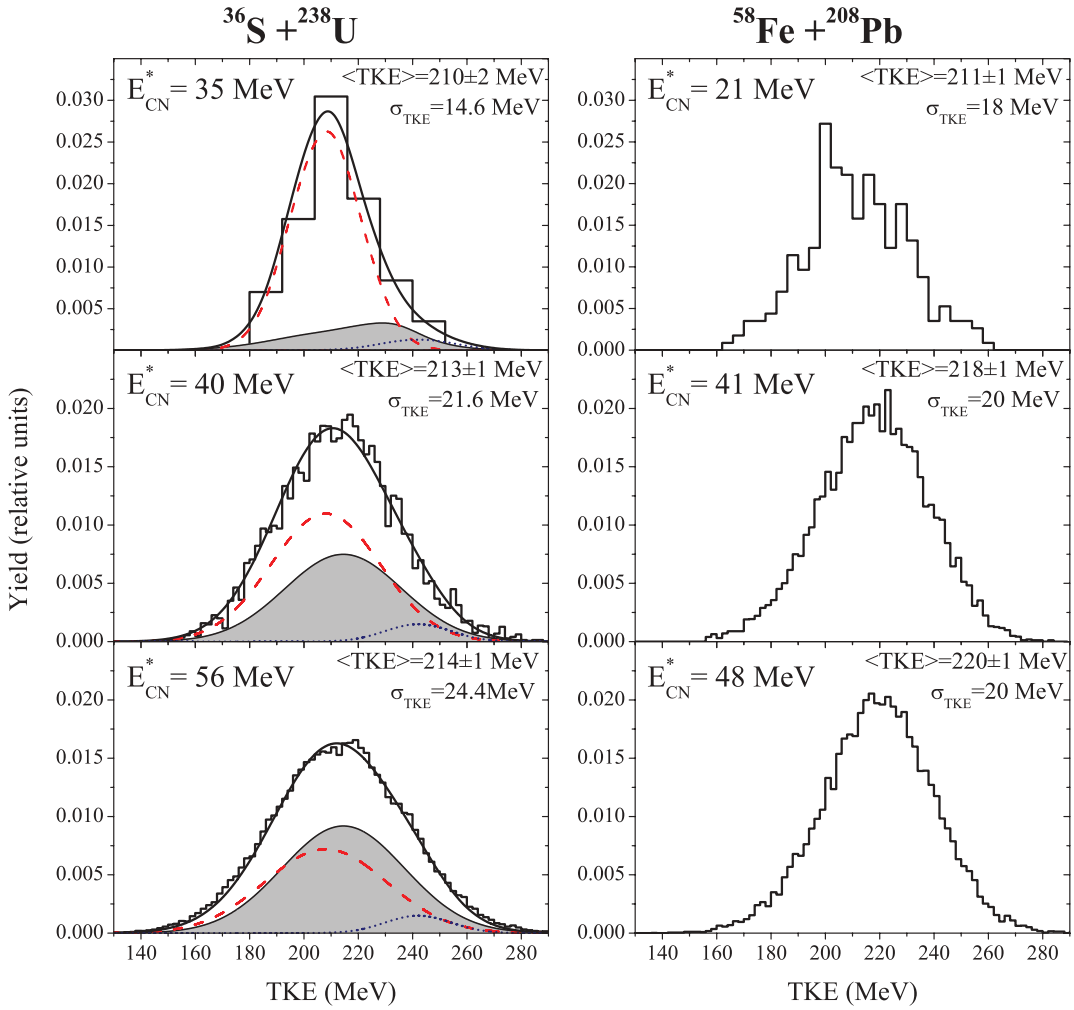

FIG. 8. (Color online) Same as Fig. 7, but for the reactions ^{36}S+^{238}U (left-hand panel) and ^{58}Fe+^{208}Pb (right-hand panel). In the case of the ^{36}S+^{238}U reaction the filled region corresponds to the TKE distribution for the CNF process with parameters taken from the ^{26}Mg+^{248}Cm reaction. The dashed and dotted curves are associated with asymmetric and symmetric QF, respectively.

was observed at the lowest excitation energy of 35 MeV, the same procedure of deconvolution was applied for the ^{36}S+^{238}U reaction at 35 MeV of excitation. The extracted CNF contribution is shown in Fig. 8 as the filled region. From the figure it is evident that at the lowest excitation energy studied the reaction is governed by the QFasym process. Moreover, in the case of ^{36}S+^{238}U, the variance of the TKE practically does not depend on fragment mass (see Fig. 5) and is equal to ∼250 MeV^2 for the whole mass range. This behavior is perfectly in line with the TKE variance observed for the reaction ^{58}Fe+^{208}Pb where the QF process is dominating. Thus, this points to the fact that the main part of fissionlike fragments originates from the QFasym process, and the contribution of other processes is relatively small at this excitation energy.

C. Fusion probability P_{CN} for reactions with ^{26}Mg and ^{36}S ions

P_{CN} is defined as the probability for CN formation from the configuration of two nuclei in contact. For these reactions the cross section of the evaporation residues (ER) is approximately a few nanobarns [35,36] and contributes insignificantly to the fusion cross section. Thus we can estimate the fusion probability using the measured mass-energy distributions as the ratio between the number of events attributed to CNF in the framework of the present analysis and all fissionlike fragments. The fusion probabilities as a function of the energy above the barrier are presented as open symbols in Fig. 9 for these reactions.

As follows from the present experimental data, the properties of the entrance channels strongly affect the reaction dynamics. At the excitation energy near the barrier the estimated values of P_{CN} are ∼70% in the case of the Mg-induced reaction and ∼25% in the S-induced reaction.

The ER cross sections for the reactions ^{26}Mg+^{248}Cm and ^{36}S+^{238}U were reported in Refs. [35] and [36]. The enhancement of sub-barrier fusion for the reaction ^{26}Mg+^{248}Cm was observed in experiment [35], caused by the orientation and coupled-channel effects on the fusion reaction with deformed targets. In the case of the ^{36}S+^{238}U reaction the sub-barrier fusion enhancement was not observed, although such an effect could be expected owing to the deformation of ^{238}U. The

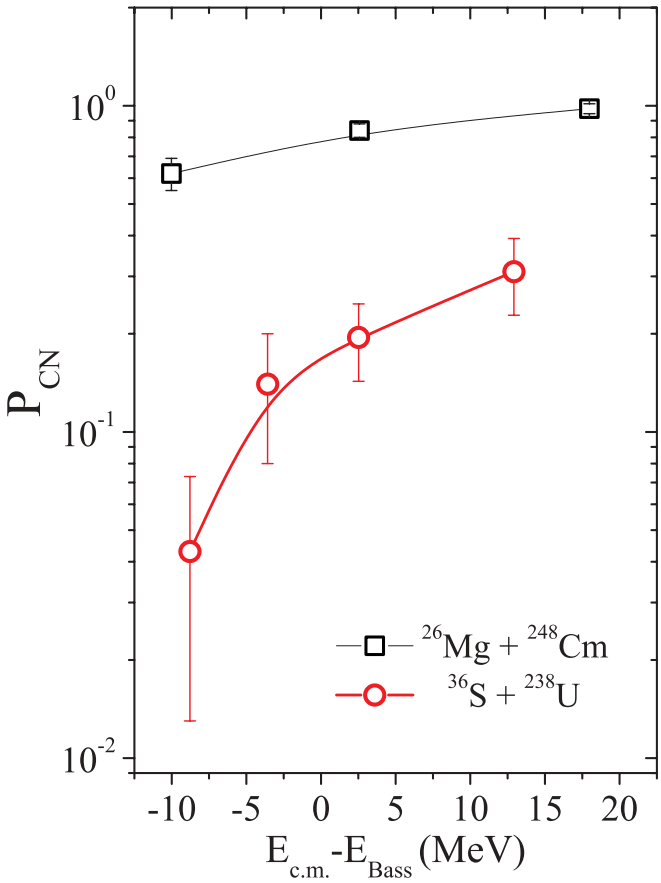

FIG. 9. (Color online) The fusion probabilities in the reactions ^{26}Mg+^{248}Cm and ^{36}S+^{238}U obtained from the present analysis of mass-energy distributions of fissionlike reaction products.

measured ER cross sections in the reaction ^{36}S+^{238}U are lower than those of the ^{26}Mg+^{248}Cm reaction. The reduction of the ER cross section for the reaction ^{36}S+^{238}U may be explained by suppression of fusion due to the dominance of the QF process as opposed to the more asymmetric ^{26}Mg+^{248}Cm reaction. Thus, as follows from the ER cross-section measurements, the fusion probability for the two reactions depends mainly on the asymmetry of the projectile-target combination. This conclusion agrees with the results of the present work.

IV. SUMMARY

The reactions ^{22}Ne+^{249}Cf, ^{26}Mg+^{248}Cm, ^{36}S+^{238}U, and ^{58}Fe+^{208}Pb have been studied to obtain information on the fusion probability as a function of the entrance channel asymmetry at energies below and above the fusion barrier. Experiments devoted to the investigation of the mass-energy distributions of binary reaction products were carried out at the FLNR Dubna using the time-of-flight spectrometer CORSET.

The properties of the measured fragment mass-energy distributions were compared with those expected for fission processes of excited CN in the framework of the liquid drop model and empirical systematics. In the case of the reaction ^{22}Ne+^{249}Cf the mass-energy distributions are in good agreement with these predictions at energies well below and above the Coulomb barrier, while for the ^{26}Mg+^{248}Cm and ^{36}S+^{238}U reactions some discrepancies between measured and predicted mass distributions were observed, especially in the asymmetric mass region. These discrepancies are connected with the QF process, whose contribution increases for the more symmetric ^{36}S+^{238}U reaction. The mass-energy distribution for the ^{58}Fe+^{208}Pb reaction has a wide U shape because QF and not CNF is the dominant process at all measured energies.

The TKE distributions for symmetric fragments with masses $A_{CN}/2\pm20$ u were analyzed for all reactions studied. It was found that the TKE distributions for the reactions ^{22}Ne+^{249}Cf and ^{26}Mg+^{248}Cm at energies well above the Coulomb barrier evolve into single Gaussians with parameters expected for the CNF process.

At a low excitation energy of 35 MeV, when shell effects should become more effective in fission, the TKE distribution of symmetric fragments obtained in the reaction ^{26}Mg+^{248}Cm differs strongly from a Gaussian shape. Besides a low-energy component, a high-energy component not foreseen in the LDM arises. This is attributed to the fact that both fission fragments are close to the spherical neutron shell $N = 82$. It means that for the compound nucleus hassium formed in the reaction ^{26}Mg+^{248}Cm the phenomenon of bimodal fission was observed for the first time.

In the case of the ^{58}Fe+^{208}Pb reaction the TKE distributions of symmetric fragments are narrower than expected for CNF. This could be a specific feature of the QF process, which should be investigated in more reactions. The mean TKE increases with excitation energy. Since for CNF the shell effects fade away with increasing excitation energy, this increase should be associated with the QF process because the QF process is colder than CNF. Therefore, shell effects still play a dominant role in QF even at relatively high excitation energies.

Furthermore, the fusion probabilities have been estimated for the two reactions ^{26}Mg+^{248}Cm and ^{36}S+^{238}U. It is found that P_{CN} is strongly enhanced in the case of the more asymmetric entrance channel, especially in the sub-barrier region.

ACKNOWLEDGMENTS

The authors would like to express their gratitude to the staff of the U400 cyclotron. This work was supported by the Alexander von Humboldt foundation and by the Russian Foundation for Basic Research (Grant No. 11-02-01507-a).

[1] R. Bock *et al.*, Nucl. Phys. A **388**, 334 (1982).
[2] J. Toke *et al.*, Nucl. Phys. A **440**, 327 (1985).
[3] W. Q. Shen *et al.*, Phys. Rev. C **36**, 115 (1987).
[4] M. G. Itkis *et al.*, Int. J. Mod. Phys. E **16**, 957 (2007).
[5] M. G. Itkis *et al.*, Nucl. Phys. A **787**, 150c (2007).
[6] G. N. Knyazheva *et al.*, Phys. Part. Nucl. Lett. **5**, 21 (2008).
[7] M. G. Itkis *et al.*, Nucl. Phys. A **734**, 136 (2004).

[8] D. J. Hinde *et al.*, Nucl. Phys. A **452**, 550 (1986).
[9] V. Zagrebaev and W. Greiner, J. Phys. G **31**, 825 (2005).
[10] V. Zagrebaev and W. Greiner, J. Phys. G **34**, 1 (2007).
[11] D. J. Hinde, M. Dasgupta, J. R. Leigh, J. C. Mein, C. R. Morton, J. O. Newton, and H. Timmers, Phys. Rev. C **53**, 1290 (1996).
[12] J. C. Mein, D. J. Hinde, M. Dasgupta, J. R. Leigh, J. O. Newton, and H. Timmers, Phys. Rev. C **55**, R995 (1997).
[13] G. N. Knyazheva *et al.*, Phys. Rev. C **75**, 064602 (2007).
[14] S. Raman, C. W. Nestor, Jr., and P. Tikkanen, At. Data Nucl. Data Tables **78**, 1 (2001).
[15] V. I. Zagrebaev *et al.* [http://nrv.jinr.ru/nrv].
[16] P. Gippner *et al.*, Z. Phys. A **325**, 335 (1986).
[17] K. Nishio *et al.*, Phys. Rev. C **82**, 024611 (2010).
[18] E. M. Kozulin *et al.*, Instrum. Exp. Tech. **51**, 44 (2008).
[19] K. Nishio *et al.*, Phys. Rev. C **77**, 064607 (2008).
[20] E. M. Kozulin *et al.*, Phys. Lett. B **686**, 227 (2010).
[21] K. Nishio *et al.*, in *Proceedings of the International Symposium on Exotic Nuclei (EXON 2009)*, edited by Yu. E. Penionzhkevich and S. M. Lukyanov, AIP Conf. Proc. No. 1224 (AIP, Melville, NY, 2009), p. 301
[22] B. B. Back *et al.*, Phys. Rev. C **53**, 1734 (1996).
[23] M. G. Itkis and A. Ya. Russanov, Fiz. Elem. Chastits At. Yadra **29**, 389 (1998) [Phys. Part. Nucl. **29**, 160 (1998)].
[24] G. Audi, A. H. Wapstra, and C. Thibault, Nucl. Phys. A **729**, 337 (2003).
[25] J. R. Nix and W. J. Swiatecki, Nucl. Phys. **71**, 1 (1965).
[26] V. E. Viola, K. Kwiatkowski, and M. Walker, Phys. Rev. C **31**, 1550 (1985).
[27] V. E. Viola, Nucl. Data Tables A **1**, 391 (1966).
[28] E. G. Ryabov, A. V. Karpov, P. N. Nadtochy, and G. D. Adeev, Phys. Rev. C **78**, 044614 (2008).
[29] P. Armbruster *et al.*, Z. Phys. A **355**, 191 (1996).
[30] E. K. Hulet *et al.*, Phys. Rev. Lett. **56**, 313 (1986).
[31] P. Möller, J. R. Nix, and W. J. Swiatecki, Nucl. Phys. A **469**, 1 (1987).
[32] M. Warda, J. L. Egido, L. M. Robledo, and K. Pomorski, Phys. Rev. C **66**, 014310 (2002).
[33] A. Staszczak, A. Baran, J. Dobaczewski, and W. Nazarewicz, Phys. Rev. C **80**, 014309 (2009).
[34] E. M. Kozulin, A. Ya. Rusanov, and G. N. Smirenkin, Phys. At. Nucl. **56**, 166 (1993).
[35] J. Dvorak *et al.*, Phys. Rev. Lett. **100**, 132503 (2008).
[36] R. Graeger *et al.*, Phys. Rev. C **81**, 061601(R) (2010).